chemosensors

Article

A Phenyl-Modified Aggregation-Induced Phosphorescent Emission-Active Cationic Ru(II) Complex for Detecting Picric Acid in Aqueous Media

Ruimin Chen †, Qinglong Zhang †, Liyan Zhang and Chun Liu *

State Key Laboratory of Fine Chemicals, Frontier Science Center for Smart Materials, School of Chemical Engineering, Dalian University of Technology, Dalian 116024, China; chenruimin@mail.dlut.edu.cn (R.C.); zhangqinglong@mail.dlut.edu.cn (Q.Z.); lyzhang@dlut.edu.cn (L.Z.)
* Correspondence: cliu@dlut.edu.cn
† These authors contributed equally to this work.

Abstract: A cationic Ru(II) complex **Ru1** with 5-phenyl-2,2′-bipyridine as ligand was synthesized and fully characterized. **Ru1** exhibits significant aggregation-induced phosphorescent emission (AIPE) activity in THF/H_2O. The AIPE property of **Ru1** has been successfully used to detect picric acid (PA) in aqueous media. **Ru1** exhibits a sensitive luminescence quenching response to PA, with a high quenching constant (K_{SV} = 2.5 × 10^4 M^{-1}) and a low limit of detection (LOD = 91 nM). In addition, **Ru1** demonstrates high sensitivity and selectivity for detecting PA in different common water samples. The UV-vis absorption spectra and luminescence lifetime of **Ru1** show an obvious change after the addition of PA into the **Ru1** samples, indicating that the quenching process is a combination of dynamic and static quenching. The density functional theory calculations indicate that the mechanism for the detection of PA is photo-induced electron transfer.

Keywords: Ru(II) complex; AIPE activity; picric acid; aqueous media; photo-induced electron transfer

Received: 9 December 2024
Revised: 6 January 2025
Accepted: 9 January 2025
Published: 11 January 2025

Citation: Chen, R.; Zhang, Q.; Zhang, L.; Liu, C. A Phenyl-Modified Aggregation-Induced Phosphorescent Emission-Active Cationic Ru(II) Complex for Detecting Picric Acid in Aqueous Media. *Chemosensors* **2025**, *13*, 14. https://doi.org/10.3390/chemosensors13010014

1. Introduction

Ru(II) complexes are considered to be an important type of phosphorescent material with high application potential due to their large Stokes shifts, visible absorption, near-infrared emission, room-temperature phosphorescence emission, and good biocompatibility [1–3]. Since ruthenium metal was reported in 1844 [4], Ru(II) complexes have been widely used in a variety of areas, including photocatalysis [5], photodynamic therapy [6], and bioimaging [7]. However, the use of Ru(II) complexes as probes is relatively rare in the detection of environmental pollutants.

In previous work, the luminescent probe has been an important application of phosphorescent materials. But when detecting biologically active molecules in physiological systems and monitoring specific ions or compounds in ecosystems, most luminescent probes exist and function in their solid or aggregated states because physiological systems and ecosystems are usually composed of aqueous solutions. This requires that solid phosphorescent materials still have good luminescence and sensing properties. However, there are few reports on the application of Ru(II) complexes in the solid or aggregated state [8].

The aggregation-caused quenching (ACQ) phenomenon severely limits the application of luminescent materials [9]. In 2001, Tang et al. reported the concept of aggregation-induced emission (AIE) [10], which provides a wider prospect for the practical application of luminescent materials. In 2002, Manimaran et al. reported the AIE phenomenon associated with Re(I) complexes and introduced the concept of aggregation-induced phosphorescent emission (AIPE) [11]. Development of the AIE and AIPE concepts provides useful guidance for the development of phosphorescent materials with good luminescence properties in their solid or aggregated state. The rotatable phenyl moiety has an important influence on the AIPE properties of the corresponding molecules [12,13]. In the single-molecule state, the excited-state energy of the molecules can be consumed by the rotation of the phenyl moiety, resulting in weak luminescence. While in the aggregated state, the phenyl moiety in the molecule is susceptible to intermolecular π-π or C-H$\cdots\pi$ interactions, leading to its rotation being blocked. Thus, the energy of the excited state of the molecule enhances the luminescence by radiative excursion, and then the AIPE phenomenon can be observed. Therefore, it is important to explore the effect of the rotatable phenyl moiety on the AIPE properties of Ru(II) complexes and to investigate its impact on the sensing performance of Ru(II) complexes as luminescent probes for practical detection.

Picric acid (PA) is an important pharmaceutical and chemical intermediate which is widely used in drug synthesis, dye manufacturing, and military industries [14]. Since PA can be dissolved in water, its leakage may cause serious pollution to the environment [15]. Long-term exposure to PA can cause headaches, anemia, and liver damage [16,17]. Therefore, it is important for human health and environmental protection to develop highly sensitive and selective methods for the detection of PA in aqueous media.

In 2022, Patra et al. reported that a Ru(II) complex with a thiophenyl-substituted 1,10-phenanthroline derivative as ligand was used for the first time in the detection of PA in CH_3CN/H_2O, with a limit of detection of 4.7 μM [18]. This suggests that Ru(II) complexes have high potential as efficient probes for detecting PA. Our group has a long-term interest in exploring the effect of structure on the properties of metal complexes and the application of metal complexes in PA detection. Recently, we have reported a series of Ir(III) and Pt(II) complexes with AIPE activities, and utilized them to achieve selective and highly sensitive detection of PA in aqueous media [19,20]. In order to further explore the effect of the phenyl moiety on the AIPE properties and the sensing performance of the detection of PA using Ru(II) complexes, we designed and synthesized a new Ru(II) complex, **Ru1**, by introducing a rotatable phenyl moiety on the 2,2′-bipyridine molecule as ligand. **Ru1** demonstrates an obvious AIPE property and excellent performance in detecting PA in THF/H_2O (Figure 1). This work reveals the influence of a phenyl moiety on the properties of Ru(II) complexes and provides better guidance for the design of high-performance Ru(II) complexes.

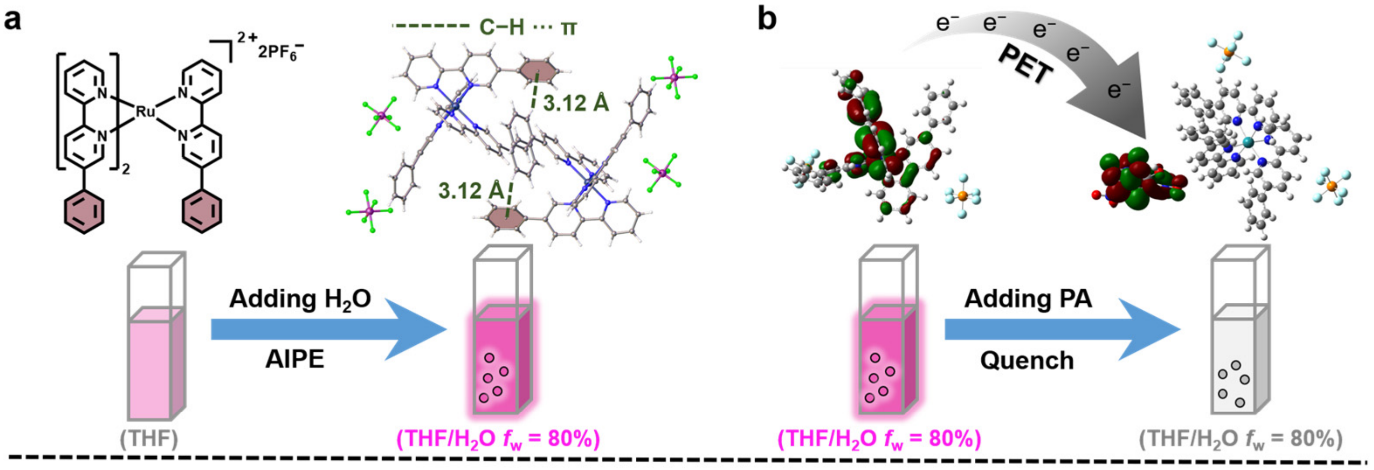

Figure 1. *Cont.*

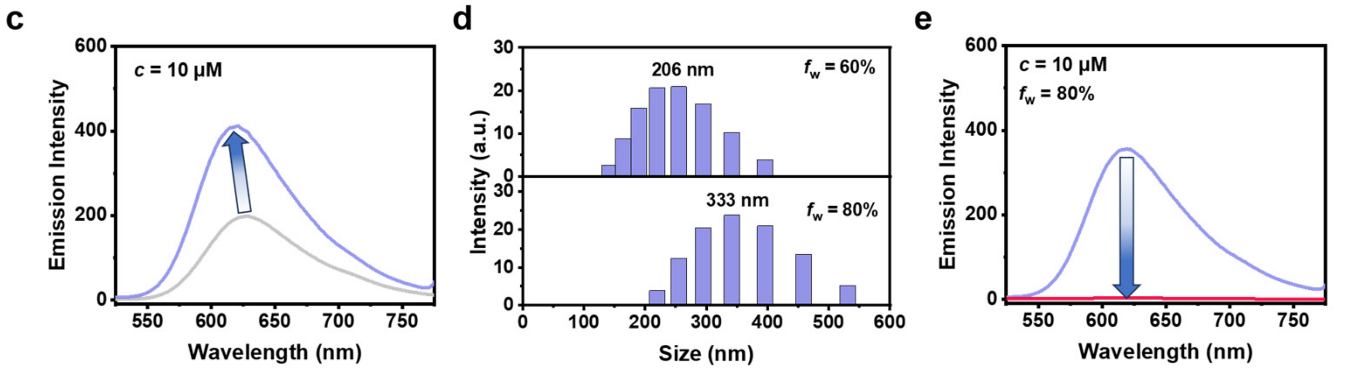

Figure 1. (**a**) Molecular formula and C−H···π intermolecular interactions in crystals of **Ru1**. (**b**) Schematic of the excited-state electrons in the LUMO of **Ru1** transferring to the LUMO of PA during quenching. (**c**) Emission spectra of **Ru1** at 0 (grey) and 80% (blue) water fractions in THF/H_2O (excitation wavelength: 400 nm). (**d**) DLS results of **Ru1** at 60% and 80% water fractions in THF/H_2O (10 μM). (**e**) Emission spectra of **Ru1** samples before (blue) and after (red) addition of PA (30 equiv.) in THF/H_2O (excitation wavelength: 400 nm).

2. Materials and Methods

2.1. Materials and Instruments

At the beginning of the experiment, all utilized materials were purchased from commercial sources and used without further purification. Mass spectra data were acquired by the Synapt G2-Si HDMS mass spectrometer (Waters, Milford, MA, USA). The ^{1}H NMR spectra were recorded using the Bruker AVANCE III 500 (Bruker, Wurzbach, Germany). The ^{13}C NMR spectra were recorded with the Bruker AVANCE NEO 400 MHz. The emission spectrum was recorded with the Hitachi F-7100 fluorescence spectrophotometer (Hitachi, Beijing, China). The absorption spectrum was recorded using an Agilent Cary 100 UV-vis spectrophotometer (Agilent, Santa Clara, CA, USA) and a Lambda 1050 + UV-vis spectrophotometer (PerkinElmer, Shanghai, China). Lifetime decay curves and absolute quantum yields (Φ) were tested using a transient/steady-state fluorescence spectrometer, FLS1000 (Edinburgh, Livingston, Scotland, UK). Scanning electron microscope (SEM) images were obtained on the field emission scanning electron microscope SEM 5000 (CIQTEK, Hefei, Anhui, China). The Malvern ZS 90 (Malvern Panalytical, Malvern, UK) was used to measure dynamic light scattering (DLS) data. The density functional theory (DFT) calculations were performed with B3LYP floods. And the LanL2DZ basis set was used for Ru atoms, while the 6-31G basis sets were applied to C atoms, H atoms, and O atoms. All calculations have been carried out using the Gaussian 16 Revision C.01.

2.2. Synthesis and Characterizations of L1 and Ru1

The ligand **L1** was synthesized using the following methods (Figure S1). A mixture of 5-bromo-2,2′-bipyridine (1.50 mmol, 352.63 mg), phenylboronic acid (2.25 mmol, 274.34 mg), potassium carbonate (3.00 mmol, 414.61 mg), tetri-(triphenylphosphine) palladium (0.03 mmol, 52.00 mg), and ethanol/water (12 mL/4 mL) was stirred at 80 °C under nitrogen for 12 h. Following cooling to room temperature, the mixture of reaction was added to deionized water (15 mL) and extracted using CH_2Cl_2 (3 × 15 mL). The ligand **L1** was finally obtained by separation and purification with basic alumina-column chromatography, using a mixture of petroleum ether and ethyl acetate (*v*/*v* 400:1 to 50:1) as the eluent.

The complex **Ru1** was prepared by a three-step process according to the synthetic route reported in the literature (Figure S1) [21,22]. In the first step, a mixture of $RuCl_3 \cdot 3H_2O$ (0.60 mmol, 156.88 mg), LiCl (3.60 mmol, 152.60 mg), ligand **L1** (1.20 mmol, 278.74 mg) and *N*,*N*-dimethylformamide (4 mL) was stirred at 165 °C under nitrogen for 6 h. Following cooling to room temperature, the mixture of reaction was added to acetone (20 mL) and stirred for 0.5 h. The mixture was then kept at −20 °C for 24 h. The solid was collected via vacuum filtration and washed with deionized water (5 × 10 mL) and ether (3 × 10 mL). After drying, the intermediate $Ru(L1)_2Cl_2$ was obtained. In the second step, a mixture of $Ru(L1)_2Cl_2$ (0.30 mmol, 190.96 mg), ligand **L1** (0.33 mmol, 76.65 mg) and ethanol/water mixture (17.5 mL/7.5 mL) was stirred at 90 °C under nitrogen for 8 h. Upon completion of the reaction, the mixture of reaction was cooled to room temperature, and vacuum evaporation of the solvent gave the crude complex. Purification of the crude complex was performed through silica gel column chromatography using an eluent consisting of acetonitrile/saturated potassium nitrate solution (*v*/*v* 200:1 to 20:1). In the third step, the purified complex obtained in step two was dissolved in a small amount of water. After adding an excess of saturated aqueous NH_4PF_6 (20 equiv.), the mixture was stirred for 2 h at room temperature. The complex **Ru1** was then obtained by filtration, rinsing with a small amount of water, and drying.

2.3. Sample Preparation and Sensing of PA

The deionized water (80 mL) was added into the solution of **Ru1** in THF (50 µmol/L, 20 mL) to prepare the suspension of **Ru1** (10 µmol/L) in THF/H_2O (*v*/*v* = 1:4). Each time, a 3 mL suspension of **Ru1** (10 µmol/L) was added to the cuvette. After the emission spectra of 11 blank samples of complex **Ru1** (THF/H_2O, *v*/*v* = 1:4, 10 µmol/L) were recorded according to the above method, the standard deviation of the emission intensity was calculated. The PA solutions were prepared in different concentrations (0.1 mmol/L to 30 mmol/L) in THF/H_2O (*v*/*v* = 1:4). After adding the solutions of different concentrations of PA (30 µL) to the samples of **Ru1** (10 µmol/L, 3 mL) in THF/H_2O (*v*/*v* = 1:4), emission and UV-vis absorption spectra were recorded. The solutions of analytes (THF/H_2O, *v*/*v* = 1:4, 30 mmol/L; nitrobenzene (NB), nitromethane (NM), 1,3-dinitrobenzene (DNB), 4-methoxyphenol (MEHQ), phenol, *p*-cresol, *m*-cresol, and 4-nitrophenol (NP)) and the solutions of compounds with different ions (THF/H_2O, *v*/*v* = 1:4, 30 mmol/L; $CuSO_4$, KF, CH_3COONa, KBr, $MnCl_2$, $MgSO_4$, $ZnCl_2$, $FeCl_2$, $CoCO_3$, $NaHCO_3$, $NiCl_2$, and $CaCl_2$) were prepared to investigate the relevant selectivity and anti-interference in the detection of PA. The selectivity- and anti-interference-property experiments were performed by the addition of the analyte solutions (30 µL) or ionic compound solutions (30 µL) to the samples of **Ru1**. The competitive experiments were conducted by adding PA (30 mmol/L, 30 µL) to the samples of **Ru1** to which were added the solutions of analytes or ionic compounds. Experiments on the performance of **Ru1** in the detection of PA in common water samples were carried out using different water samples for the preparation of the complex samples (THF/H_2O, *v*/*v* = 1:4), including river water (Lingshui River, Dalian, China), tap water (Dalian University of Technology, Dalian, China), rainwater (Dalian University of Technology, Dalian, China), and deionized water. The solution of PA (30 mmol/L, 30 µL) was added to samples of **Ru1** (THF/H_2O, *v*/*v* = 1:4, 10 µmol/L) prepared with different water samples and the emission spectra were recorded.

3. Results and Discussion

3.1. AIPE Properties of Ru1

The normalized emission and UV-vis absorption spectra of **Ru1** in THF at room temperature are shown in Figure S2. Similar to most Ru(II) complexes [23], the strong absorption band of **Ru1** at 275–375 nm is attributed to the ligand-centered (LC) π-π^* transition. The weak absorption band between 400–500 nm is attributed to a metal-to-ligand charge transition (MLCT) and a ligand-to-ligand charge transition (LLCT). The photophysical data of **Ru1** are shown in Table S1.

The emission spectra of **Ru1** in THF/H_2O with different water fractions were tested (Figure 2). The emission intensity of the **Ru1** sample gradually increases as the water fraction is increased from 0–70%. With the continued increase of the water fraction to 80%, the emission intensity of the sample reaches the maximum, indicating that **Ru1** has a significant AIPE property. This may be due to the aggregation of **Ru1** as the water fraction increases, leading to the locking of the rotatable phenyl moiety in the ligand and the increase of emission intensity [24]. To prove this hypothesis, DLS tests of **Ru1** samples in THF/H_2O were performed. As shown in Figure 1d and Figure S3a, the average sizes of the aggregates are 206 nm, 224 nm, and 333 nm at 60%, 70%, and 80% water fractions, respectively. The results show that **Ru1** molecules aggregate with increases in the water fraction, and the average size of the aggregates gradually increases. In addition, an SEM image of **Ru1** in THF/H_2O with a water fraction of 80% also shows that **Ru1** molecules aggregate and form nanoparticles (Figure S3b).

A single crystal of **Ru1** was cultured by the slow diffusion of ether into the solution of **Ru1** in acetone and studied in detail by single-crystal X-ray diffraction analysis (Figure S4). The crystal-related data for **Ru1** are shown in Tables S2–S4. As shown in Figure 3a,b, there are abundant C-H$\cdots\pi$ intermolecular interactions, with distances of 3.12 Å and 3.25 Å between the complex molecules (the burgundy plane represents the π plane). The fluorine atoms of the PF_6^- ions also form a large number of C-H$\cdots$F intermolecular interactions with hydrogen atoms in the cationic part of the complex (Figure 3c–e). Thus, the intermolecular C-H$\cdots\pi$ and C-H$\cdots$F interactions lock the rotatable phenyl moiety in the ligand, which leads to increased emission intensity in the aggregated state. Furthermore, two layers of cations are sandwiched between two layers of anions along the [001] direction (Figure S5). The ordered arrangement of anions with the cations suggests that electrostatic interaction also plays a crucial role in the stacking of the molecules.

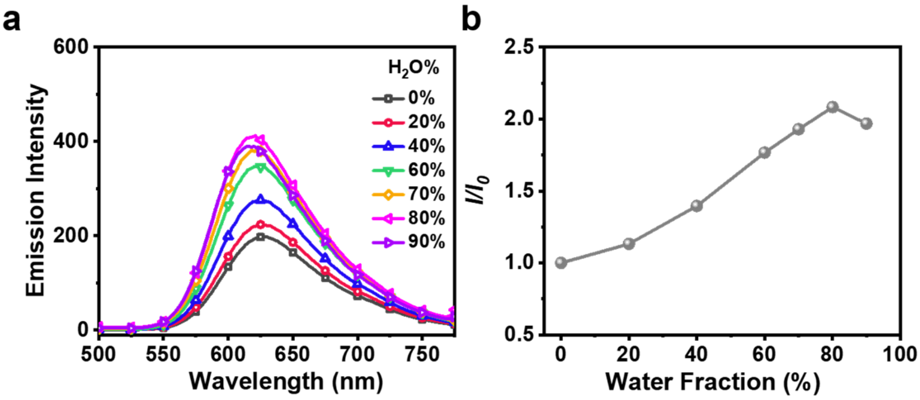

Figure 2. (**a**) Emission spectra of **Ru1** samples (THF/H_2O, 10 μmol/L) with different water fractions (excitation wavelength: 400 nm). (**b**) The plot of emission intensity ratio (I/I_0) of **Ru1** samples versus the different water fractions (f_w) of THF/H_2O.

3.2. Detection of PA

The AIPE activity of **Ru1** in THF/H_2O prompted us to use **Ru1** as a luminescent probe to detect PA in aqueous media. Therefore, we performed luminescence quenching experiments for **Ru1** in THF/H_2O (v/v = 1:4) with the addition of different concentrations of PA. The emission intensity of the **Ru1** sample obviously decreases with increases in the concentration of the PA solutions (Figure 4a,b). The quenching efficiency of the **Ru1** sample is 50.7% after addition of PA at a concentration of 30 μM. When the concentration of PA is 200 μM, the quenching efficiency of **Ru1** sample reaches 97.4%.

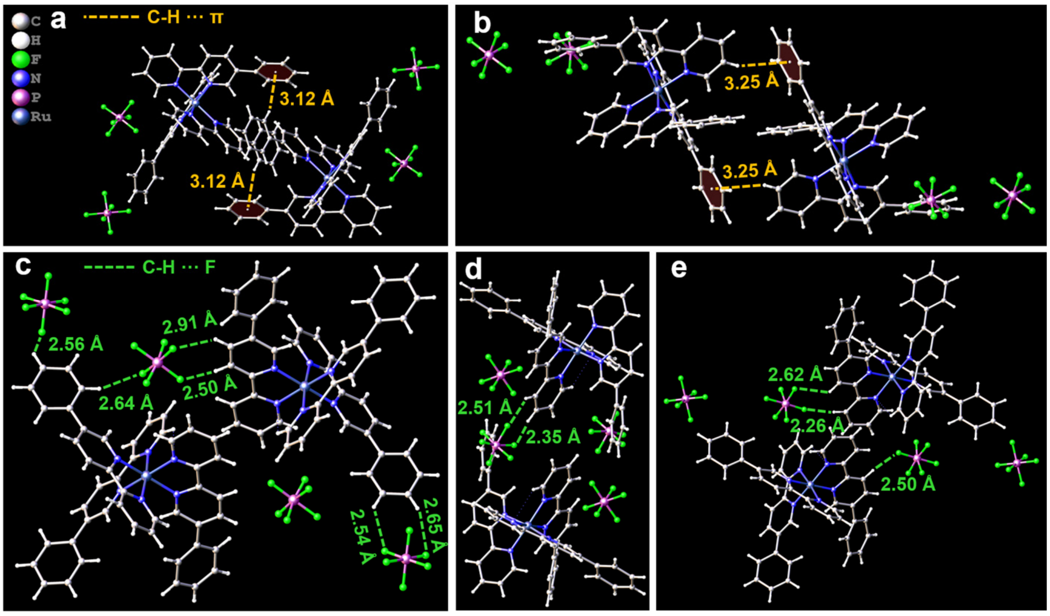

Figure 3. (**a**,**b**) C-H···π interactions and (**c**–**e**) C-H···F interactions between **Ru1** molecules in a single crystal.

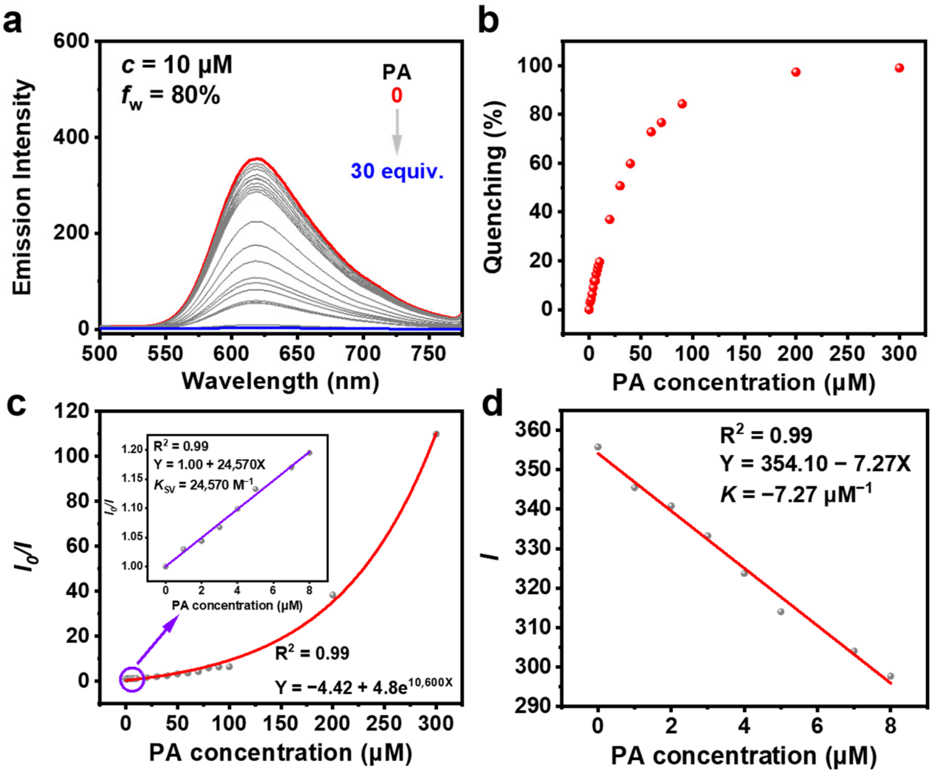

Figure 4. (**a**) Emission spectra of **Ru1** in THF/H_2O with the addition of different concentrations of PA (excitation wavelength: 400 nm). (**b**) Quenching efficiencies of **Ru1** after the addition of different concentrations of PA. (**c**) The Stern–Volmer plot of I_0/I vs. the concentration of PA. Inset: The linear part of the Stern–Volmer plot at a low-concentration range of PA. (**d**) Linear plot of emission intensities of **Ru1** vs. the concentration of PA.

To further analyze the sensitivity of **Ru1** in the detection of PA, the correlations between I_0 and I (I_0 and I represent the emission intensities of **Ru1** samples without PA and after the addition of different concentrations of PA, respectively) and [Q] (the molar concentration of PA) were fitted, and a Stern–Volmer plot was obtained (Figure 4c). With the addition of PA in a low-concentration range (0–8 μM), the Stern–Volmer plot exhibits good linearity. However, as the concentration of PA continues to increase, the Stern–Volmer plot gradually deviates from linearity, which may be due to the presence of both dynamic quenching and static quenching in the process of luminescence quenching [25]. The sensitivity of **Ru1** for the detection of PA was further analyzed by the Stern–Volmer equation $I_0/I = K_{SV}[Q] + 1$ in the PA concentration range of 0–8 μM. The quenching constant (K_{SV}) is 2.5×10^4 M^{-1}. The limit of detection (LOD) was calculated according to the formula LOD = $3\sigma/K$, where σ represents the standard deviation of the emission intensities of the blank samples (Figure S6 and Table S5), and K represents the slope of the linear relationship between the emission intensities and the concentrations of PA (Figure 4d). The LOD was calculated to be 91 nM, which is much lower than that of the Ru(II) complex previously reported [18]. These results indicate that **Ru1** has good performance in detecting PA in aqueous media.

In order to explore whether **Ru1** has good selectivity and anti-interference properties in the detection of PA, the luminescence response of **Ru1** was studied for several common analytes (nitrobenzene (NB), nitromethane (NM), 1,3-dinitrobenzene (DNB), 4-methoxyphenol (MEHQ), phenol, *p*-cresol, *m*-cresol, and 4-nitrophenol (NP)) and ionic compounds ($CuSO_4$, KF, CH_3COONa, KBr, $MnCl_2$, $MgSO_4$, $ZnCl_2$, $FeCl_2$, $CoCO_3$, $NaHCO_3$, $NiCl_2$, and $CaCl_2$). Based on the results in Figures 5a,b and S7a,b, the emission intensities of the **Ru1** samples do not change significantly after the addition of different analytes (30 equiv.) and ionic compounds (30 equiv.). When PA (30 equiv.) was added to the **Ru1** samples with different ionic compounds and analytes, the quenching efficiencies of the samples were significantly increased, and all exceeded 98%. In summary, **Ru1** has good selectivity and anti-interference properties and a low LOD, compared to other previously reported Ru(II), Ir(III), and Pt(II) complexes, for the detection of PA in aqueous media (Table S6).

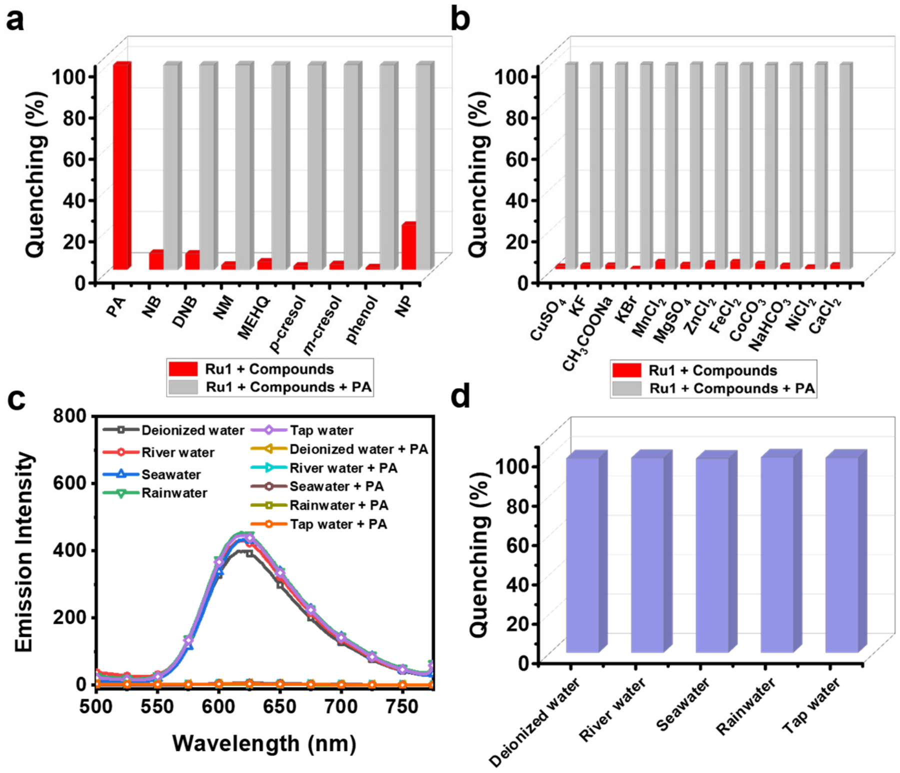

Figure 5. (**a**) Quenching efficiencies of **Ru1** with the addition of different analytes in THF/H_2O (v/v = 1:4), before (red) and after (gray) the addition of PA (30 equiv.). (**b**) Quenching efficiencies of **Ru1** with addition of different ionic compounds in THF/H_2O (v/v = 1:4), before (red) and after (gray) the addition of PA (30 equiv.). (**c**) Emission spectra of **Ru1** in different water samples (excitation wavelength: 400 nm). (**d**) Quenching efficiency of **Ru1** with PA (30 equiv.) in different water samples.

To promote the application of **Ru1**, the ability of **Ru1** to detect PA in real environments was further evaluated. The deionized water in the THF/H_2O was replaced by river water, seawater, rainwater and tap water, respectively. Subsequently, the emission spectra of the **Ru1** samples prepared in these common water samples were tested. The results in Figure 5c show that the emission spectra of **Ru1** samples prepared in the common water samples were similar to those from the deionized-water samples. As shown in Figure 5d, the quenching efficiencies of the **Ru1** samples prepared using different common water samples were over 98% after the addition of PA (30 equiv.). As a result, it was determined that **Ru1** can be used as an efficient luminescent probe for the detection of PA in real environmental water samples.

3.3. Sensing Mechanism

To better understand the quenching process, the luminescence lifetimes of **Ru1** samples with the addition of different concentrations of PA were investigated (Figure S8). The luminescence lifetime of the **Ru1** sample decreases significantly after the addition of the PA solution, indicating that there is dynamic quenching during the quenching process [26]. Furthermore, τ_0/τ and the molar concentration of PA are fitted (τ_0 and τ are the luminescence lifetimes without and after the addition of PA, respectively), and they show a good linear relationship (Figure 6a). The results show that there is dynamic quenching after the addition of PA at the high and low concentration ranges. In addition, the UV-vis absorption spectra of the **Ru1** samples with the addition of different concentrations of PA were investigated (Figure 6b). The absorption peaks, at 307 nm and 457 nm, of the **Ru1** samples were gradually shifted with increasing concentrations of PA, and a new absorption band around 357 nm was generated. These results indicate that static quenching also occurs during the quenching process, and there are strong interactions between **Ru1** and PA [27]. Therefore, both dynamic quenching and static quenching occurred during the luminescence quenching of the **Ru1** samples.

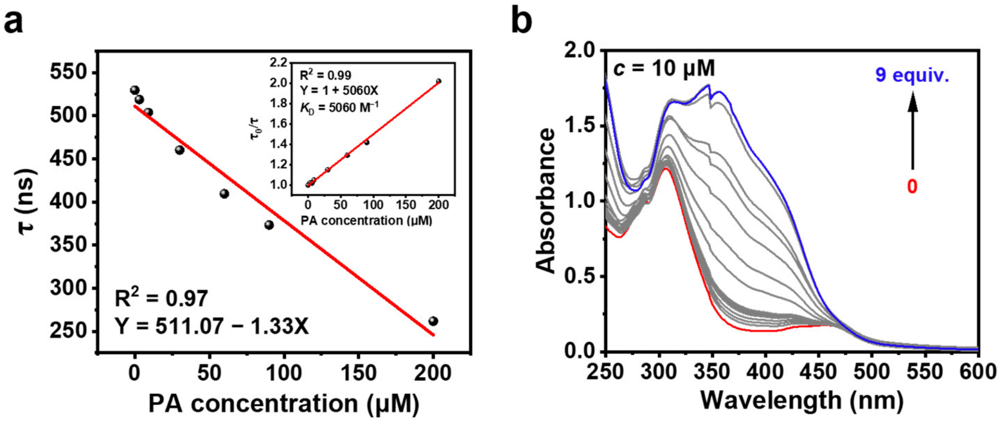

Figure 6. (**a**) Variation in the luminescence lifetime (τ) of **Ru1** samples after addition of different concentrations of PA solutions in THF/H_2O (v/v = 1:4). Inset: ratio of luminescence lifetime (τ_0/τ) of **Ru1** samples before (τ_0) and after (τ) the addition of different concentrations of PA, as a function of the concentration of the PA solution. (**b**) UV-vis absorption spectra of **Ru1** samples with the addition of different concentrations of PA in THF/H_2O (v/v = 1:4).

Furthermore, the absence of overlap between the UV-vis absorption spectra of PA and the emission spectra of **Ru1** in THF/H_2O with a water fraction of 80% (Figure 7a) suggests that there is no Förster resonance energy transfer during the luminescence quenching of **Ru1** [28,29]. In the ^1H NMR spectra, there is no significant change in the proton signal of **Ru1** after the addition of PA, suggesting that PA does not lead to the decomposition of **Ru1** (Figure S9). Due to the decrease in the luminescence lifetime of the **Ru1** samples after the addition of PA, the cause of the luminescence quenching of the **Ru1** samples could be photo-induced electron transfer (PET) [30,31]. To prove this conjecture, the relevant density-functional theory (DFT) calculations were performed on **Ru1**, PA, and the adduct (**Ru1** + PA). From the results in Figure 7b, it can be seen that LUMO energy of PA (−3.49 eV) is much lower than that of **Ru1** (−2.48 eV), which indicates that the excited-state electrons in the LUMO of **Ru1** can be easily transferred to the LUMO of PA during the quenching process. This implies that PET occurs between **Ru1** and PA, leading to luminescence quenching of the **Ru1** samples [26,32]. These results show that **Ru1** can achieve high sensitivity detection of PA mainly due to the PET.

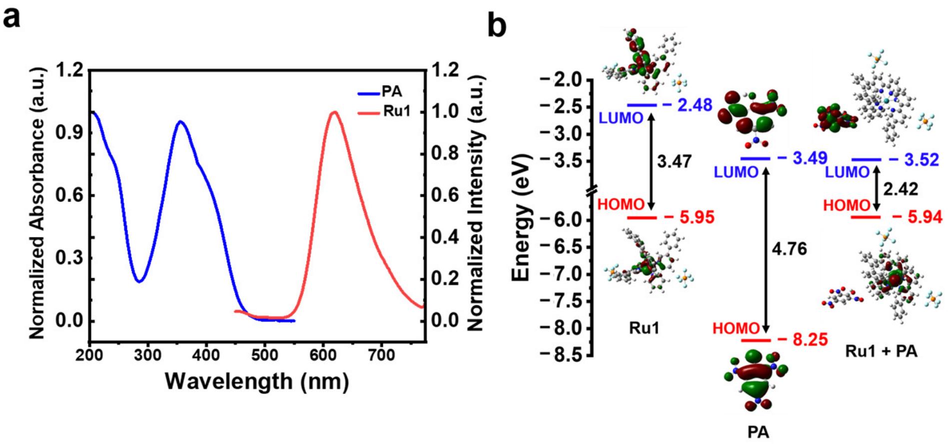

Figure 7. (**a**) Normalized emission spectra of **Ru1** (red) and normalized UV-vis absorption spectra of PA (blue). (**b**) Energy level diagrams of **Ru1**, PA, and the adduct (**Ru1** + PA), obtained from theoretical calculations.

4. Conclusions

In this work, a new cationic Ru(II) complex **Ru1** with AIPE activity was synthesized by introducing a rotatable phenyl moiety on the 2,2′-bipyridine as ligand to investigate the effect of a rotatable phenyl moiety on the AIPE properties, and the detection properties for PA, of the Ru(II) complex. The rotatable phenyl moiety has an important effect on the AIPE properties of the **Ru1**, as its rotation is restricted by intermolecular C-H$\cdots\pi$ and C-H$\cdots$F interactions in the aggregated state. When the AIPE activity of **Ru1** is utilized for the detection of PA, **Ru1** achieves highly sensitive and selective detection of PA, with a low LOD of 91 nM, in aqueous media. In addition, the quenching process is a combination of dynamic quenching and static quenching, and the mechanism for the detection of PA is attributed to PET. These findings reveal the influence of a phenyl moiety on the properties of Ru(II) complexes and provide a better guidance for the design of high-performance Ru(II) complexes.

Supplementary Materials: The following supporting information can be downloaded at: https://www.mdpi.com/article/10.3390/chemosensors13010014/s1. Figure S1: Synthesis routes of ligand **L1** and **Ru1**; Figure S2: Normalized UV-vis absorption and emission spectra of **Ru1** in THF (solid line: absorption spectrum; dashed line: emission spectrum; excitation wavelength: 400 nm); Figure S3: (a) DLS analysis of **Ru1** in THF/H_2O at a 70% water fraction, (b) SEM image of **Ru1** aggregates in THF/H_2O at an 80% water fraction; Figure S4: The crystal structure of **Ru1**; Figure S5: Molecular stacking in the crystal structure of **Ru1** (gold dashed-line: C-H$\cdots\pi$ intermolecular interactions, green dashed-line: C-H$\cdots$F intermolecular interactions); Figure S6: Emission spectra in 11 blank samples (THF/H_2O, v/v = 1:4, 10 μmol/L) of **Ru1** with excitation wavelength of 400 nm; Figure S7: (a) Emission spectra of **Ru1** samples (THF/H_2O, v/v = 1:4, 10 μmol/L) after addition of different analytes (30 equiv.) with excitation wavelength of 400 nm. (b) Emission spectra of **Ru1** samples

(THF/H_2O, v/v = 1:4, 10 µmol/L) after addition of different ionic compounds (30 equiv.) with excitation wavelength of 400 nm; Figure S8: Luminescence lifetime decay curves for **Ru1** samples (THF/H_2O, v/v = 1:4, 10 µmol/L) after addition of different concentrations of PA solutions in THF/H_2O (v/v = 1:4); Figure S9: The ^1H NMR spectra of **Ru1**, PA and **Ru1** + PA in DMSO-d_6; Figure S10: The ^1H NMR spectra of **L1** in $CDCl_3$; Figure S11: The ^1H NMR spectrum of **Ru1** in DMSO-d_6; Figure S12: The ^{13}C NMR spectrum of **Ru1** in DMSO-d_6; Figure S13: The HRMS of the cationic portion of **Ru1**; Figure S14: The HRMS of the anionic portion of **Ru1**; Table S1: Photophysical properties of **Ru1**; Table S2: Single-crystal data for the complex **Ru1**; Table S3: C-H$\cdots\pi$ interaction data in the complex **Ru1**; Table S4: C-H$\cdots$F interaction data in crystals of the complex **Ru1**; Table S5: Emission intensity at 619 nm of 11 blank samples of the complex **Ru1** (THF/H_2O, v/v = 1:4, 10 µmol/L); Table S6: Some reported metal complexes for the detection of PA. References [18,33–40] are cited in the supplementary materials.

Author Contributions: Investigation, R.C. and Q.Z.; Data curation, Visualization, Writing—original draft, R.C.; Formal analysis, R.C., Q.Z. and L.Z.; Writing—review and editing, R.C., Q.Z., L.Z. and C.L.; Resources, C.L.; Funding acquisition, Supervision, C.L. All authors have read and agreed to the published version of the manuscript.

Funding: This work was supported by the National Natural Science Foundation of China (21978042) and the Fundamental Research Funds for the Central Universities (DUT22LAB610).

Institutional Review Board Statement: Not applicable.

Informed Consent Statement: Not applicable.

Data Availability Statement: Data are contained within the article.

Conflicts of Interest: The authors declare no conflicts of interest.

References

1. Kar, B.; Das, U.; Roy, N.; Paira, P. Recent advances on organelle specific Ru(II)/Ir(III)/Re(I) based complexes for photodynamic therapy. *Coord. Chem. Rev.* **2023**, *474*, 214860. [CrossRef]
2. Fernandes, R.S.; Ch, S.; Ghosh, B.; Dey, N. Sulfide-induced concentration-dependent distinct optical response: Unique chromogenic probe developed for analyzing fecal contamination in water and intracellular imaging applications. *ACS Sustain. Chem. Eng.* **2024**, *12*, 4922–4932. [CrossRef]
3. Wang, Z.; Gao, Y.; He, Z.; Lu, L. Aggregation-induced electrochemiluminescence-active ruthenium(II) complex for selective detection of dopamine. *J. Electroanal. Chem.* **2023**, *947*, 117783. [CrossRef]
4. Higgins, S. Regarding ruthenium. *Nat. Chem.* **2010**, *2*, 1100. [CrossRef]
5. Watson, E.E.; Russo, F.; Moreau, D.; Winssinger, N. Optochemical control of therapeutic agents through photocatalyzed isomerization. *Angew. Chem. Int. Ed.* **2022**, *61*, e202203390. [CrossRef]
6. Wu, Q.; Yuan, C.; Wang, J.; Li, G.; Zhu, C.; Li, L.; Wang, Z.; Lv, Q.; Mei, W. Uridine-modified ruthenium(II) complex aslysosomal LIMP-2 targeting photodynamic therapy photosensitizer for the treatment of triple-negative breast cancer. *JACS Au* **2024**, *4*, 1081–1096. [CrossRef]
7. Ramu, V.; Wijaya, L.S.; Beztsinna, N.; Van de Griend, C.; van de Water, B.; Bonnet, S.; Le Dévédec, S.E. Cell viability imaging in tumor spheroids via DNA binding of a ruthenium(ii) light-switch complex. *Chem. Commun.* **2024**, *60*, 6308–6311. [CrossRef]
8. Gao, Y.; Wang, Z.; Wu, J.; Lu, L. A cellular NO sensor based on aggregation-induced electrochemiluminescence and photoelectron transfer of a novel ruthenium(II) complex. *Microchem. J.* **2023**, *190*, 108714. [CrossRef]
9. Hong, Y.; Lam, J.W.Y.; Tang, B.Z. Aggregation-induced emission. *Chem. Soc. Rev.* **2011**, *40*, 5361–5388. [CrossRef]
10. Luo, J.; Xie, Z.; Lam, J.W.Y.; Cheng, L.; Chen, H.; Qiu, C.; Kwok, H.S.; Zhan, X.; Liu, Y.; Zhu, D.; et al. Aggregation-induced emission of 1-methyl-1,2,3,4,5-pentaphenylsilole. *Chem. Commun.* **2001**, 1740–1741. [CrossRef]
11. Manimaran, B.; Thanasekaran, P.; Rajendran, T.; Lin, R.-J.; Chang, I.J.; Lee, G.-H.; Peng, S.-M.; Rajagopal, S.; Lu, K.-L. Luminescence enhancement induced by aggregation of alkoxy-bridged rhenium(I) molecular rectangles. *Inorg. Chem.* **2002**, *41*, 5323–5325. [CrossRef]
12. Chen, J.; Law, C.C.W.; Lam, J.W.Y.; Dong, Y.; Lo, S.M.F.; Williams, I.D.; Zhu, D.; Tang, B.Z. Synthesis, light emission, nanoaggregation, and restricted intramolecular rotation of 1,1-substituted 2,3,4,5-tetraphenylsiloles. *Chem. Mater.* **2003**, *15*, 1535–1546. [CrossRef]

13. Mei, J.; Hong, Y.; Lam, J.W.Y.; Qin, A.; Tang, Y.; Tang, B.Z. Aggregation-induced emission: The whole is more brilliant than the parts. *Adv. Mater.* **2014**, *26*, 5429–5479. [CrossRef]
14. Ejaz, M.; Mohamed, M.G.; Kuo, S.-W. Fluorescent benzoxazine–perylene linked covalent organic polymer as a sensing probe for lead ions and 2,4,6-trinitrophenol. *ACS Appl. Polym. Mater.* **2024**, *6*, 9170–9179. [CrossRef]
15. Suhendra, N.F.; Sharma, R.; Lee, H.-i. Thermally versatile maleimide-based polymeric thin film for detection and separation of picric acid from polluted areas. *Sens. Actuators B Chem.* **2024**, *418*, 136345. [CrossRef]
16. Huo, T.; Yang, B.; He, Y. New porous organic framework Py-PDA CHOF as fluorescent chemosensor for detecting 2,4,6-trinitrophenol in environmental samples. *Microchem. J.* **2024**, *205*, 111271. [CrossRef]
17. Dhiman, S.; Singla, N.; Ahmad, M.; Singh, P.; Kumar, S. Protonation- and electrostatic-interaction-based fluorescence probes for the selective detection of picric acid (2,4,6-trinitrophenol)—An explosive material. *Mater. Adv.* **2021**, *2*, 6466–6498. [CrossRef]
18. Patra, S.K.; Sen, B.; Rabha, M.; Khatua, S. An aggregation-induced emission-active bis-heteroleptic ruthenium(ii) complex of thiophenyl substituted phenanthroline for the selective "turn-off" detection of picric acid. *New J. Chem.* **2022**, *46*, 169–177. [CrossRef]
19. He, P.; Chen, Y.; Li, X.-N.; Yan, Y.-Y.; Liu, C. Aggregation-induced emission-active iridium(III) complexes for sensing picric acid in water. *Chemosensors* **2023**, *11*, 177. [CrossRef]
20. Yan, Y.; Jia, W.; Cai, R.; Liu, C. An AIPE-active fluorinated cationic Pt(II) complex for efficient detection of picric acid in aqueous media. *Chin. Chem. Lett.* **2024**, *35*, 108819. [CrossRef]
21. Marmion, M.E.; Takeuchi, K.J. Ruthenium(IV)-oxo complexes: The novel utilization of tertiary pnicogen ligands. *J. Am. Chem. Soc.* **1988**, *110*, 1472–1480. [CrossRef]
22. Yang, X.-J.; Janiak, C.; Heinze, J.; Drepper, F.; Mayer, P.; Piotrowski, H.; Klüfers, P. Heteroleptic 5,5-disubstituted-2,2-bipyridine complexes of ruthenium(II): Spectral, electrochemical, and structural investigations. *Inorg. Chim. Acta* **2001**, *318*, 103–116. [CrossRef]
23. Wei, L.; He, X.; Zhao, D.; Kandawa-Shultz, M.; Shao, G.; Wang, Y. Biotin-conjugated Ru(II) complexes with AIE characteristics as mitochondria-targeted photosensitizers for enhancing photodynamic therapy by disrupting cellular redox balance. *Eur. J. Med. Chem.* **2024**, *264*, 115985. [CrossRef]
24. Di, L.; Xing, Y.; Yang, Z.; Qiao, C.; Xia, Z. Photostable aggregation-induced emission of iridium(III) complex realizing robust and high-resolution imaging of latent fingerprints. *Sens. Actuators B Chem.* **2023**, *375*, 132898. [CrossRef]
25. Thippeswamy, M.S.; Naik, L.; Maridevarmath, C.V.; Savanur, H.M.; Malimath, G.H. Studies on the characterisation of thiophene substituted 1,3,4-oxadiazole derivative for the highly selective and sensitive detection of picric acid. *J. Mol. Struct.* **2022**, *1264*, 133274. [CrossRef]
26. Zu, F.; Yan, F.; Bai, Z.; Xu, J.; Wang, Y.; Huang, Y.; Zhou, X. The quenching of the fluorescence of carbon dots: A review on mechanisms and applications. *Microchim. Acta* **2017**, *184*, 1899–1914. [CrossRef]
27. Shi, Z.; Li, W.; Pi, H.; Liu, H.; Chen, H.; Li, P.; Jiang, X. Trace amounts of mercaptans with key roles in forming an efficient three-component photoinitiation system for holography. *Mater. Today Chem.* **2022**, *26*, 100999. [CrossRef]
28. P, K.; Cherian, A.R.; Sirimahachai, U.; Thadathil, D.A.; Varghese, A.; Hegde, G. Detection of picric acid in industrial effluents using multifunctional green fluorescent B/N-carbon quantum dots. *J. Environ. Chem. Eng.* **2022**, *10*, 107209. [CrossRef]
29. Yang, X.; Liu, W.; Liu, X.; Sun, Y.; Wang, X.; Shao, Y.; Liu, W. Construction of multifunctional luminescent lanthanide MOFs for luminescent sensing of temperature, trifluoroacetic acid vapor and explosives. *Inorg. Chem.* **2024**, *63*, 3921–3930. [CrossRef]
30. Escudero, D. Revising intramolecular photoinduced electron transfer (PET) from first-principles. *Acc. Chem. Res.* **2016**, *49*, 1816–1824. [CrossRef]
31. Sharma, A.; Enderlein, J.; Kumbhakar, M. Photon antibunching reveals static and dynamic quenching interaction of tryptophan with Atto-655. *J. Phys. Chem. Lett.* **2017**, *8*, 5821–5826. [CrossRef] [PubMed]
32. Ouyang, T.; Guo, X.; Cui, Q.; Zhang, W.; Dong, W.; Fei, T. Conjugated polymer nanoparticles based on anthracene and tetraphenylethene for nitroaromatics detection in aqueous phase. *Chemosensors* **2022**, *10*, 366. [CrossRef]
33. Kuleshova, O.; Asako, S.; Ilies, L. Ligand-enabled, iridium-catalyzed ortho-borylation of fluoroarenes. *ACS Catal.* **2021**, *11*, 5968–5973. [CrossRef]
34. Malik, S.; Mondal, U.; Jana, N.C.; Banerjee, P.; Saha, A. Using eugenol scaffold to explore the explosive sensing properties of Cd(ii)-based coordination polymers: Experimental studies and real sample analysis. *Dalton Trans.* **2024**, *53*, 12995–13011. [CrossRef]
35. Xu, J.; Zhang, L.; Shi, Y.; Liu, C. Carbazolyl-modified neutral Ir(III) complexes for efficient detection of picric acid in aqueous media. *Sensors* **2024**, *24*, 4074. [CrossRef] [PubMed]
36. Ghosh, S.; Mukherjee, P.S. Self-assembly of a nanoscopic prism via a new organometallic Pt3 acceptor and its fluorescent detection of nitroaromatics. *Organometallics* **2008**, *27*, 316–319. [CrossRef]
37. Hou, Y.; Shi, R.; Yuan, H.; Zhang, M. Highly emissive perylene diimide-based bowtie-shaped metallacycles. *Chin. Chem. Lett.* **2023**, *34*, 107688. [CrossRef]

38. Ma, Q.; Dong, W.; Ma, Z.; Lv, X.; Li, Y.; Duan, Q. Synthesis of phosphorescent iridium(III) complex containing carbazole and its sensing property towards nitro-aromatic compounds. *Mater. Lett.* **2019**, *249*, 120–123. [CrossRef]
39. Dong, W.; Ma, Q.; Ma, Z.; Duan, Q.; Lü, X.; Qiu, N.; Fei, T.; Su, Z. Phosphorescent iridium(III) complex based photoluminescence sensor for sensitive and selective detection of picric acid. *Dyes Pigm.* **2020**, *172*, 107799. [CrossRef]
40. Yi, S.; Lu, Z.; Xie, Z.; Hou, L. Amphiphilic gemini-iridium (III) complex for rapid and selective detection of picric acid in water and intracellular. *Talanta* **2020**, *208*, 120372. [CrossRef]